



Faraday  
Discussions

**Catalytic Activation of Molecular Nitrogen for Green  
Ammonia Synthesis: Introduction and Current Status**

Journal:	<i>Faraday Discussions</i>
Manuscript ID	FD-ART-03-2023-000070.R1
Article Type:	Paper
Date Submitted by the Author:	05-Apr-2023
Complete List of Authors:	Hosono, Hideo; Tokyo Institute of Technology, Materials and Structures Laboratory

SCHOLARONE™  
Manuscripts

## ARTICLE

## Catalytic Activation of Molecular Nitrogen for Green Ammonia Synthesis: Introduction and Current Status

Hideo Hosono<sup>a,b</sup>

Received 00th January 20xx,  
Accepted 00th January 20xx

DOI: 10.1039/x0xx00000x

The efficient synthesis of ammonia using carbon footprint-free hydrogen at mild conditions is a grand challenge in chemistry today. Novel concepts are needed for the activation process and catalyst to achieve this objective. This article briefly reviews catalytic activation of N<sub>2</sub> for ammonia synthesis at mild conditions. The features of the various activation methods reported so far are summarized, looking chronologically back at progress in heterogeneous catalysts since iron oxide for Haber-Bosch process, and finally the technical challenges to be overcome are described. Establishing low work functions for the support materials of the metal catalysts is one key to reducing the activation barrier to dissociate N<sub>2</sub> bonding. Surfaces of electronegative materials that preserve the character of the bulk are shown to be useful for this purpose. The requirements of desired catalysts are high efficiency at low temperatures, Ru-free compositions, and chemical robustness in ambient atmosphere.

### 1. Introduction

Nitrogen is an indispensable element for life and a key constituent for various materials, as well as fine chemicals. Nitrogen molecules occupy ~80 % of the atmosphere, but are chemically inert due to the strength of the N-N triple bond and absence of polarity. Thus, it was a great challenge in chemistry to activate N<sub>2</sub> from its artificial transformation into chemically usable molecules, such as NH<sub>3</sub> and NO<sub>x</sub>. The establishment of the Haber · Bosch (HB) method in 1913 marked the first successful chemical process of nitrogen fixation, saving the human civilization from a hunger crisis. Since then, the HB process for synthesizing NH<sub>3</sub> from N<sub>2</sub> and H<sub>2</sub> has been the predominant method for industrial NH<sub>3</sub> production up to now.

The annual production of NH<sub>3</sub> has increased to 170 million tons globally, which making it the second most mass-produced chemical. The chemical equilibrium underlying this process is given in eq. 1.

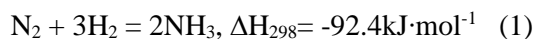


Figure 1 shows the equilibrium NH<sub>3</sub> concentration as a function of reaction temperature and pressure.

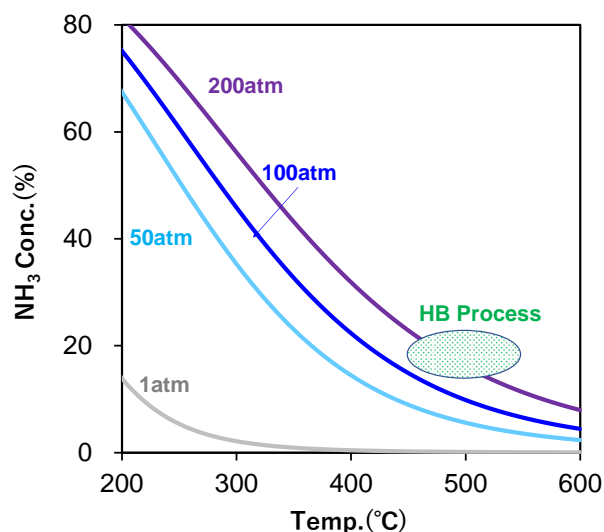
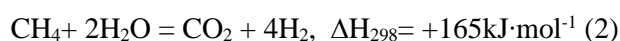


Fig.1 Equilibrium NH<sub>3</sub> concentration

The lower temperature and the higher pressure, the higher is the obtained NH<sub>3</sub> concentration. However, the energy barrier for dissociation of the N-N triple bond, corresponding to the rate determining step (RDS) of the process, is high. A catalyst is thus required to lower the energy barrier. The industrial HB process adopts iron-based oxides as the catalyst and is operated at 450–550 °C and 20–40 MPa, with the resulting the production being ~20 % NH<sub>3</sub>. The H<sub>2</sub> for the reaction is produced from the methane steam reforming and water gas shift reactions (eq. 2).



<sup>a</sup> MDX Research Centre for Element Strategy, International Research Frontiers Initiative, Tokyo Institute of Technology, Midori, Yokohama 226-8503, JAPAN  
<sup>b</sup> WPI-mana, National Institute for Materials Science, Tsukuba 305-0044, JAPAN  
information available should be included here. See DOI: 10.1039/x0xx00000x

This reaction is endothermic and needs a large input of energy, especially as ammonia is so mass-produced (170 million ton per year). Consequently, the HB process has grown to encompass 1-2% of the total global energy consumption. However, the ammonia synthesis process in eq.1 itself is energy-efficient thanks to the combination of an endothermic reaction (2) and an exothermic reaction (1).

Recently, ammonia synthesis is becoming subject to new demand, i.e., for green ammonia. The HB process is accompanied by CO<sub>2</sub> emission as H<sub>2</sub> is obtained by eq. 2. The reduction of the carbon footprint of this process is a requirement that must be met. As such, the focus is on H<sub>2</sub> derived from water electrolysis driven by renewable energy derived from solar and wind power. Another key technical challenge to realizing green ammonia is the creation of high-performance catalysts and/or novel production processes which efficiently work even at mild conditions (low temperature and low pressure). In addition, in order for the HB process to be cost effective, huge amounts of ammonia are produced at large-scale plants. Green ammonia process offers the opportunity of using a small-scale plant for on-site production where ammonia is required and/or H<sub>2</sub> can be available as a by-product.

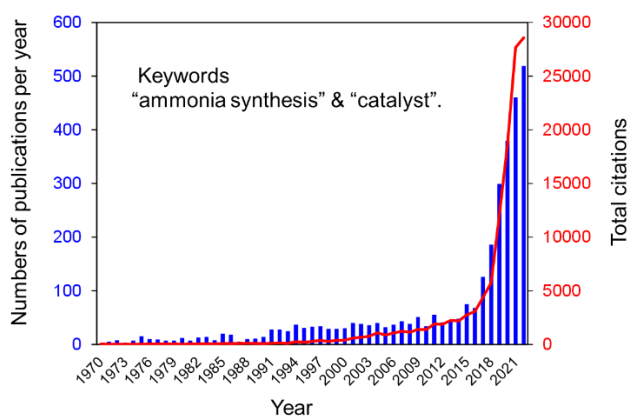


Fig.2. Statistics of publication number and citation of the topic of ammonia synthesis. Data source: web of science.

Figure 2 shows the variation in the number of research papers on catalysts for ammonia synthesis and their citation numbers with year since 1970. It is evident the activity in the last decade has steeply increased to date.

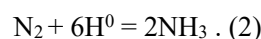
This trend reflects these recent social demands that strongly drive intensive research on sustainable nitrogen activation. In this article, I describe the general picture of catalytic ammonia synthesis through the activation of molecular nitrogen as the introduction and the status of heterogeneous catalysts for green ammonia synthesis. Since so many publications on this subject have accumulated so far, I'm afraid my literature survey for this article is incomplete. The readers are encouraged to refer to the monographs and review articles cited in reference <sup>1-9</sup>.

## 2.General Picture of N<sub>2</sub> activation

The general scheme for NH<sub>3</sub> synthesis from N<sub>2</sub> activation may be expressed by the following equation (1):



Since the combination of H<sup>+</sup> (proton) and an electron may be regarded as H<sup>0</sup>, the following route is also possible:



Since H<sup>0</sup> may be created from H<sup>-</sup> (hydride) as well by detaching an electron, efficient NH<sub>3</sub> formation is achievable using metal-loaded metal hydrides. The multiple common oxidation states of hydrogen, from cationic to neutral and anionic, makes it possible to achieve NH<sub>3</sub> formation through different N<sub>2</sub> activation routes and mechanisms.

Figure 3 shows the general scheme of green ammonia synthesis consisting of the production of H<sub>2</sub>/energy, the NH<sub>3</sub> synthesis process, and its applications. A variety of processes suitable for NH<sub>3</sub> synthesis at mild conditions are now known. Table 1 summarizes these catalytic ammonia synthetic processes, along with the advantages and current issues for each one. These processes are classified into chemistry-based and physics-based methods according to the way N<sub>2</sub> is activated. N<sub>2</sub> excitation can be achieved by various energy sources and excitation modes. The plasma process is a typical physical excitation tool. Here, an energetic electron corresponding to several thousand Kelvin excites vibrational states of N<sub>2</sub> in the gas phase and adsorbed on the catalysis, improving NH<sub>3</sub> formation efficiency (Fig.4a). Combining this plasma approach with catalysts not only improves the efficiency but also leads to the activity of the precious metal Ru being surpassed by the non-precious metals Ni and Co, as shown in Fig.4b.<sup>10,11</sup>

## ARTICLE

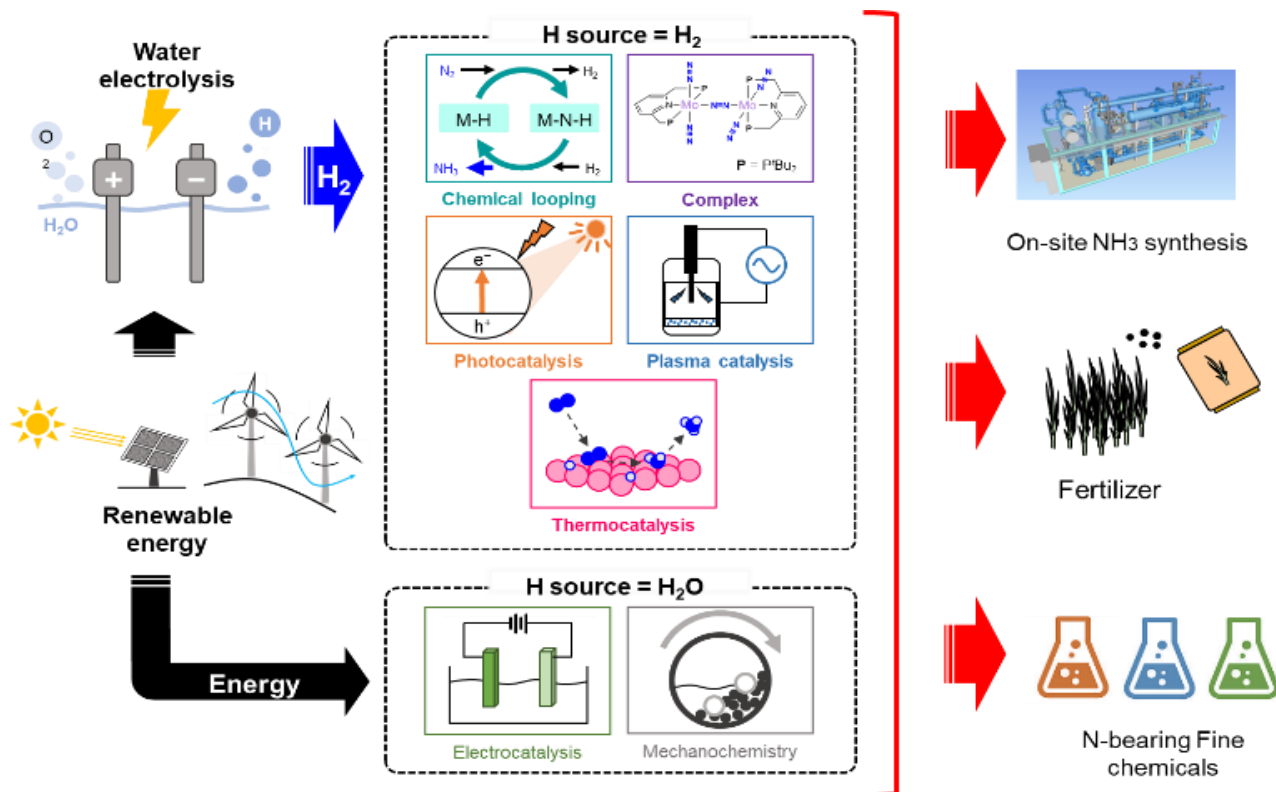
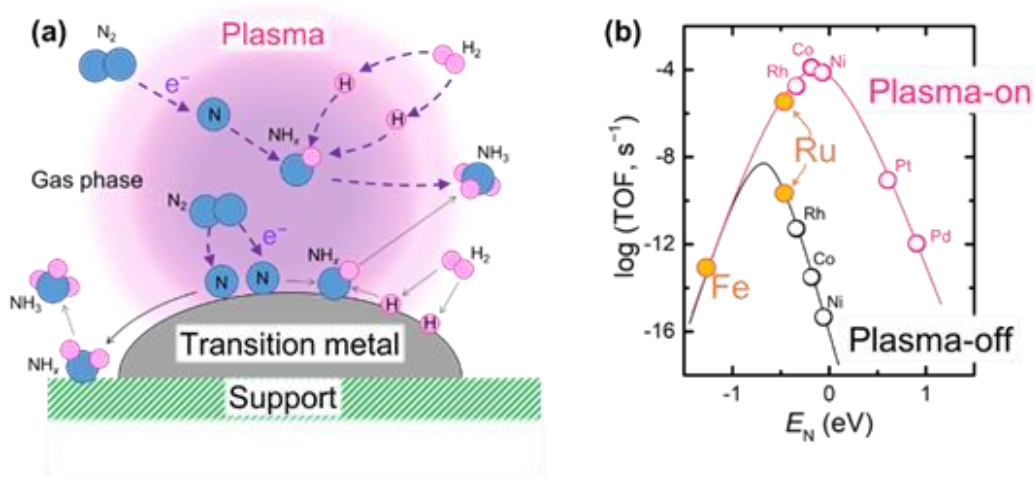


Fig.3 Green ammonia synthesis and applications

Fig.4 Schematic plasma catalysis. The optimal catalytic metal shifts from Ru to Co(Ni) upon plasma-on<sup>10</sup>

## ARTICLE

Table 1. Various methods for catalytic ammonia synthesis at mild condition

Method	N <sub>2</sub> activation	Advantages	Challenges	Example
Thermal catalysis	Heat + Catalyst	1-step process, Practical for commercial plant	Attaining equilibrium at mild conditions, Ru-free, active catalyst	Ru-Cs/MgO
Chemical looping	Separation of N <sub>2</sub> and H <sub>2</sub> activation	High selectivity, Beyond Sabatier relation	2-step process	Ni/LiH
Mechano catalysis	Shear stress + frictional heat	No external heating, H <sub>2</sub> O as H source	Low efficiency, 2-step process	Iron ball milling in N <sub>2</sub> + subsequent reaction with H <sub>2</sub> O/H <sub>2</sub>
Electrocatalysis	Electron injection from metallic cathode	RT synthesis, H <sub>2</sub> O as H-source	Low efficiency due to competitive H <sub>2</sub> evolution	Wide variety of metals
Photocatalysis	Transfer of photo-generated electron on semiconductor	RT synthesis	Low efficiency (band gap excitation and energy transfer to N <sub>2</sub> )	Doped TiO <sub>2</sub>
Non-equilibrium plasma catalysis	Excitation of N <sub>2</sub> vibrational state in gas phase and on catalyst by high temp. electron	RT synthesis, Beyond equilibrium limit and Sabatier relation	Electricity cost Reaction vessel design	Transition metal + LT plasma
Complex catalyst	Capturing N <sub>2</sub> on unsaturated site transition metal complex	RT synthesis, H <sub>2</sub> O as proton source, Well-defined active site	Cost Reductant is needed	Organo Mo-complex + SmI <sub>2</sub> (reductant)

## ARTICLE

Research on electrocatalytic  $\text{NH}_3$  synthesis is recently extremely active. The essence of this method is the cathodic reduction of  $\text{N}_2$  molecules on a metallic conducting electrode.<sup>12,13</sup> An advantage of this method is that water is usable as a proton source at RT. However, the reduction potential of  $\text{N}_2$  is more negative to that of  $\text{H}_2$  evolution from water (Fig.5a). This is the primary obstacle to improving the Faraday efficiency of  $\text{NH}_3$  synthesis. Photocatalysis adopts semiconductors instead of metals as the catalyst, and photo-generated electrons are used to reduce  $\text{N}_2$  molecules as is illustrated for the case of  $\text{TiO}_2$  in Fig.5b

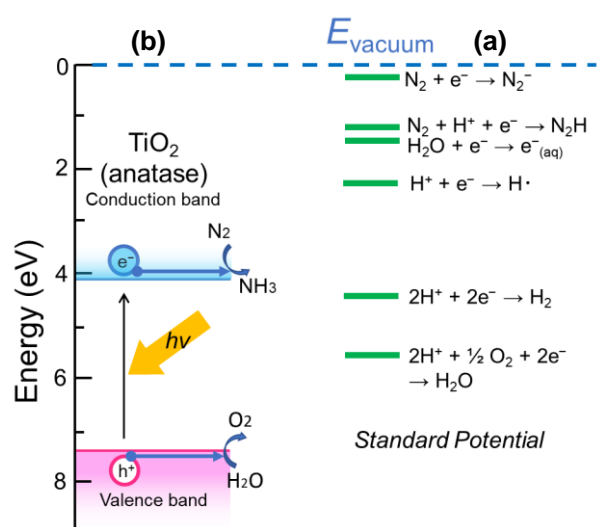


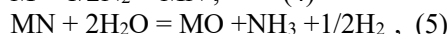
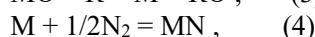
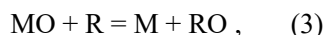
Fig.5 Standard potential of relevant reduction reactions (a) and energy level of  $\text{TiO}_2$  for photocatalysis (b). The vacuum level is set at the origin.

Photo-excited plasmons may also be used for the activation of  $\text{N}_2$  adsorbed on metal surfaces.<sup>14</sup> In each method, the efficiency is determined by the photogeneration of electrons/plasmons and the subsequent activation of adsorbed  $\text{N}_2$  with the resulting electrons/electric field.

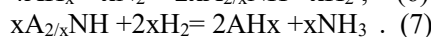
Mechanochemical catalysis for  $\text{NH}_3$  synthesis was first reported in 2020.<sup>15</sup> The advantages for this approach are its operation at RT and simple experimental setup. First,  $\text{N}_2$  is activated by mechanical stress and frictional heat generated by ball milling with iron balls. Subsequently, this activated  $\text{N}_2$  species on the iron ball is converted to  $\text{NH}_3$  by reaction with  $\text{H}_2/\text{H}_2\text{O}$ .<sup>16,17</sup> Although higher concentrations of ammonia exceeding that of the HB process can be obtained, the process is 2-step, and the formation rate is rather slow. Thus, the energy efficiency for  $\text{NH}_3$  synthesis appears to be very low, and thus this method is likely to be not suitable for

practical application, although the way of activating  $\text{N}_2$  is novel.

Chemical looping (CL) catalysis<sup>18</sup> consists of separated processes for the activation of  $\text{N}_2$  and the reaction of activated  $\text{N}_2$  (nitrides) with  $\text{H}_2$ . The general formula of CL for  $\text{NH}_3$  synthesis is described by the following schemes:



where M and R denote an active metal and a reducing agent, respectively. The advantages of the CL approach to  $\text{NH}_3$  synthesis are operation at atmospheric pressure, high selectivity of  $\text{NH}_3$  formation, and surpassing the limits of the equilibrium  $\text{NH}_3$  concentration in (1). The first CL approach to  $\text{NH}_3$  synthesis was reported by Chen's group<sup>19</sup>, with the use of alkali/alkaline earth (A) hydrides to perform the following reactions;



The formation of the imide  $\text{A}_2\text{NH}$  is the key to activation of  $\text{N}_2$ . Please note the valence state of hydrogen changes from -1 (hydride) to 0 ( $\text{H}_2$ ) and +1 ( $\text{NH}_3$ ) in this CL process. Late transition metals (Fe, Co and Ni) were employed as effective catalysts for both steps. The drawbacks of this CL looping process are that it is a 2-step process and that  $\text{AH}$  and  $\text{A}_2\text{NH}$  are rather sensitive to the ambient atmosphere.

Complex catalysis is performed in homogeneous system. Mo-based complex with an unsaturated coordination site is used mimicking the active site in nitrogenase. This catalysis is a fundamental study on  $\text{NH}_3$  synthesis because a definite active site can be designed. Usage of water/alcohol was achieved as the H-source while the stoichiometric reducing agents such as  $\text{SmI}_2$  is required.<sup>20,21</sup>

### 3. Progress in heterogeneous catalysts for thermal $\text{NH}_3$ synthesis

Thermal processes using heterogeneous catalysts are likely to be most practical methods for  $\text{NH}_3$  synthesis with respect to cost and efficiency. However, novel highly efficient and stable catalysts are required for green  $\text{NH}_3$  synthesis because the iron-based catalysts used for the HB process are not so active under the mild conditions demanded by this

approach. In this section, the progress in heterogeneous catalysts for this purpose is described chronically. Figure 6 depicts the mile-stones in this progress beyond the iron-

based catalysts. The catalyst for the industrial HB process was established as  $\text{Fe}_3\text{O}_4:\text{K}_2\text{O}+\text{Al}_2\text{O}_3$  (Swedish Ore), which

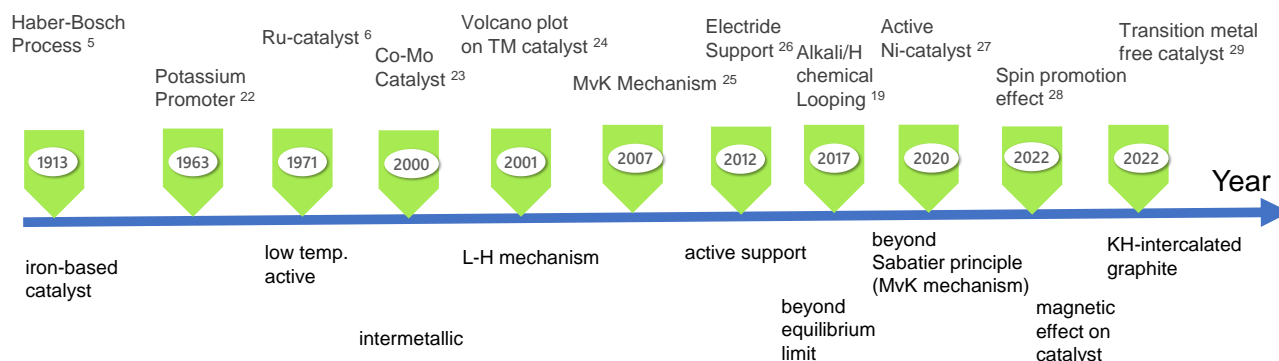


Fig.6 Progress in heterogeneous catalysts for  $\text{NH}_3$  synthesis

was reached by Mittasch et al through extensive screening endeavors.<sup>1,2,5</sup> Although several modifications have been made, iron oxide-based materials have been applied to the present day. Since iron oxides are reduced to metallic iron under the conditions of  $\text{NH}_3$  synthesis, iron bearing  $\text{K}_2\text{O}$  and  $\text{Al}_2\text{O}_3$  may be effective catalysts for the HB process in practice. The exploration of new catalysts toward  $\text{NH}_3$  synthesis under mild conditions began with this material. In

1963, the activity enhancement by the addition of potash ( $\text{K}_2\text{CO}_3$ ) to an iron catalyst was reported.<sup>22</sup> This finding provides a clue the reason why Swedish iron ore exhibits excellent activity. In 1971 Ozaki et al.<sup>6</sup> discovered that ruthenium promoted with metallic alkali works well for  $\text{NH}_3$  synthesis at lower temperatures. Since then, Ru has been used as the primary catalyst for  $\text{NH}_3$  synthesis at mild conditions in place of

### 3.1. Transition metal catalysts

Since the dissociation energy of  $\text{N}_2$  is much larger than that of  $\text{H}_2$ , reducing the energy barrier of  $\text{N}_2$  dissociation is the key strategy for artificial  $\text{NH}_3$  synthesis. When the N-N bond dissociation process occurs as the rate determining step on the surface of a transition metal particle loaded on a support, i.e. following the Langmuir-Hinshelwood (LH) Mechanism, a clear relation is found between the  $\text{N}_2$  chemisorption energy and the catalytic activity. Figure 7 shows the well-known “volcano plot” relationship (an expression of the more general Sabatier principle) reported in 2001 by the Nørskov group.<sup>24</sup> According to this plot, the optimal catalysts are group 8 elements (Fe, Ru, and Os), each of which was already demonstrated to be effective (Os was the catalyst Haber used for his first successful ammonia synthesis).<sup>1-4</sup> Molybdenum is located in a non-optimal region because its interaction with N is too strong, but

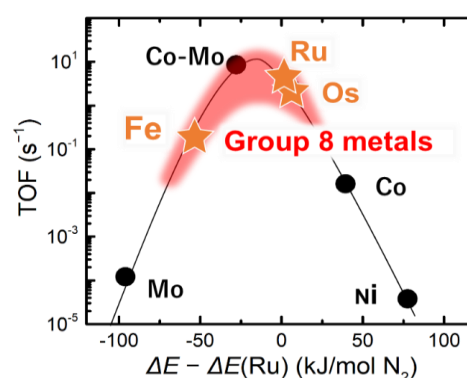


Fig.7 Turnover frequency (TOF) of  $\text{NH}_3$  synthesis vs. adsorption energy of nitrogen on transition metal<sup>24</sup>

its combination with Co from the opposite side of the plot, in the form of the intermetallic phase  $\text{Mo}_3\text{Co}_3\text{N}$ <sup>22</sup>

exhibits higher activity, demonstrating the validity of this volcano relation. However, since in practice  $\text{NH}_3$  synthesis is carried out at high pressures to enhance the formation rate and the outlet concentration of  $\text{NH}_3$ , this is an obstacle that needs to be overcome.

Another drawback of Ru is its high cost, which reflects its low natural abundance. To escape the Sabatier relation (volcano plot), it is necessary to shift the mechanism for  $\text{N}_2$  dissociation as the rate determining step away from the LH-type scheme. The higher activity of Co-Mo-nitride catalysts over iron-based catalysts is understood in terms of nitrogen adsorption via a Mars-van Krevelen (MvK) mechanism, in which  $\text{N}_2$  activation occurs not at a Co/Mo site but at a surface nitrogen vacancy site.<sup>30,31</sup> This is due to change in mechanism from the LH (dissociative) to MvK(associative)-type process invites the utilization of non-precious transition metals which are far from the optimal position in the volcano plot.<sup>31</sup> A representative example will be Ni-loaded metal nitrides.<sup>27</sup> As predicted from the volcano plot, the catalytic activity of Ni is very low in general. However, Ni-loaded LaN or CeN exhibits high activity comparable to conventional Ru-loaded catalysts, and the activation energy ( $\sim 50\text{kJmol}^{-1}$ ) becomes almost half that of the Ru-catalysts. Measurement using isotopically labelled  $^{15}\text{N}_2$ , kinetic analysis, and high-resolution STEM observations on the surface revealed that a lot of nitrogen vacancies are formed on the surface and that  $\text{N}_2$  molecules are activated not on the loaded Ni but on these N-vacancies. Figure 8 shows the schematic mechanism for this process supported by the DFT calculations. In this case, the role of the loaded transition metal is just  $\text{H}_2$ -dissociation which is much easier than  $\text{N}_2$ , so even Ni works well for this purpose

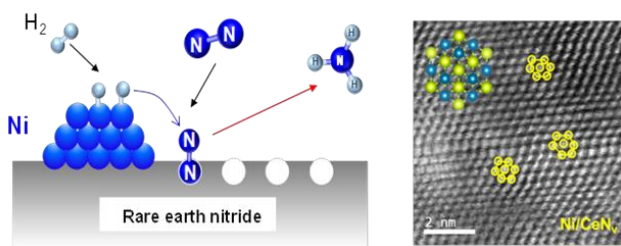


Fig.8 Schematic mechanism for  $\text{NH}_3$  synthesis on Ni/Rare earth nitride. HAADF-STEM images show local distortion due to N-vacancy on the surface after the treatment of Ni/CeN under  $\text{H}_2$  at  $400^\circ\text{C}$ .<sup>27</sup>

### 3.2 Promoters and active supports

The discovery of a pronounced promotion effect of alkali carbonates added to iron and ruthenium catalysts highlighted the role and state of these promoters. The role of promoters is classified into two types, based on whether they carry out electronic or structural actions.  $\text{Al}_2\text{O}_3$  and  $\text{K}_2\text{O}$  in the Mitsunobu catalyst are prototypes of structural and electronic promoters, respectively. The former enhances the numbers of active sites, while the latter promotes electron donation to the iron catalyst.

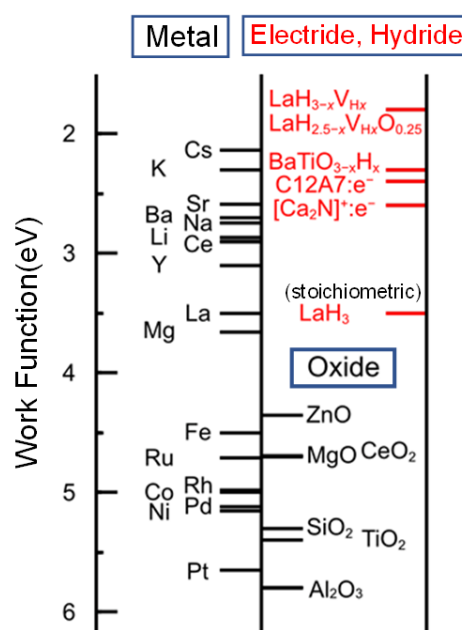


Fig.9 Work function of relevant metal, oxide and active support (electride and hydride)

Here, we focus on electronic promotion. The dissociation of  $\text{N}_2$  molecules adsorbed on supported transition metal nanoparticles is enhanced by electron donation from the promoters. Ozaki<sup>6</sup> connected the ammonia formation rate on a Ru catalyst to the electronegativity of the alkali/alkaline-earth oxide promoters. The work function ( $\phi$ ) is an appropriate physical parameter to express the potential of electron donation from one material to others. Materials with low ( $\phi$ ) have been examined as supports since a stable inorganic electride C12A7:e<sup>-</sup> was discovered with  $\phi=2.4\text{eV}$ . These materials not only serve as a simple

support to enhance the dispersion of transition metal particles but also work as electronic promoters. That is, the combination of a low work function support with transition metal particles functions as a single entity catalyst. Thus, we hereafter refer to these supporting materials with low work function as *active supports*. Figure 9 summarizes the work functions of relevant metals and active support materials. It is noted from the figure that the work functions of transition metals are distinctly larger than those of the active supports. In general, electron transfer across the interface between an (n-type) semiconductor and a metal is controlled by two factors: the work function difference ( $\phi_M - \phi_{\text{semi}}$ ) between the metal and semiconductor, and the carrier concentration of the semiconductor. Since the  $\phi_M$  of transition metals is rather larger than the  $\phi_{\text{semi}}$  values, the contact should be Schottky-type having an energy barrier height corresponding to  $\phi_M - \phi_{\text{semi}}$ , as illustrated in Fig.10. This means electron transfer from the active support/promotor to the metal catalyst is

the catalytic activity is rarely explicitly examined, because few support materials have electron concentrations that can be controlled over a wide range.

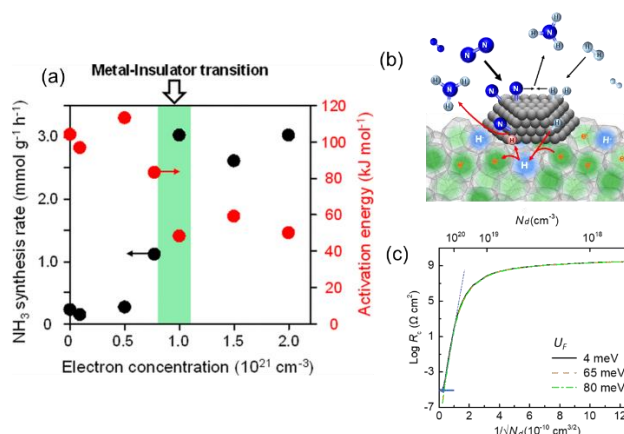


Fig.11 (a) Catalytic activity as a function of carrier electron concentrations in C12A7:e<sup>-</sup>. (b) catalytic mechanism, and (c) contact resistance  $R_c$  between Ru.C12A7:e<sup>-</sup> as a function of carrier concentration  $N_e$ .  $U_f = E(\text{cond. band min.}) - \text{Fermi level}$ , ---- indicates the slope predicted by tunneling mechanism ( $\log R_c \propto 1/\sqrt{N_d}$ )

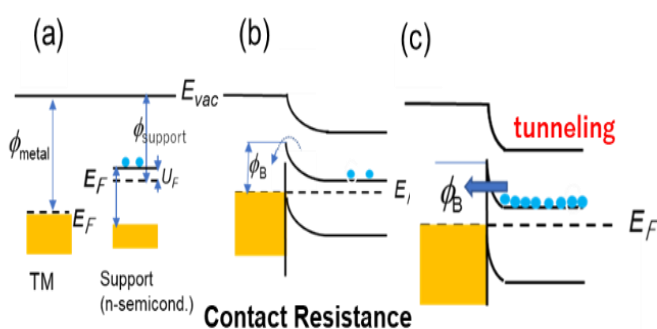


Fig.10 Energy band diagram of transition metal (TM) and support (n-type semiconductor) before contact, (b) after contact. Schottky barrier with height= $\phi_{\text{TM}} - \phi_{\text{support}}$  is formed.  $\Phi$ ;work function. (c) when electron carrier concentration is high, electrons pass through thinned barrier by tunnelling.<sup>32</sup>

largely suppressed by this barrier. However, as the electron concentration is increased in the semiconductor (support), the barrier width becomes thinner. When the width becomes sufficiently thin, electrons can pass through the barrier to the metal via the tunnelling mechanism. The effect of carrier concentration in the support/promotor on

Figure 11 (a) shows one of the exceptions with the relation between carrier electron concentration ( $N_e$ ) in C12A7:e<sup>-</sup> and the activation ( $E_a$ ) of  $\text{NH}_3$  synthesis by Ru/C12A7:e<sup>-</sup> at 400°C-0.1MPa.<sup>33</sup> C12A7:e<sup>-</sup> is one of the first stable electride materials. It is derived from the chemical composition 12CaO·7Al<sub>2</sub>O<sub>3</sub> (C12A7), and its electrical conduction that can be controllably tuned from insulating to metallic with a maximal  $N_e$  of  $\sim 2 \times 10^{21}$  cm<sup>-3</sup>.<sup>34</sup> The  $E_a$  in the semiconducting region remains  $\sim 100$  kJ mol<sup>-1</sup>, which is similar to that for conventional supports such as MgO, but reduces to  $\sim 50$  kJ mol<sup>-1</sup> in the metallic region. This drastic change originates from a switch of the rate determining step from N<sub>2</sub> dissociation on Ru to N-H bond formation caused by enhanced electron donation from C12A7:e<sup>-</sup> to N<sub>2</sub> adsorbed on Ru. Fig.11(b) shows the contact resistance between C12A7:e<sup>-</sup> and Ru as a function of  $N_e$  in C12A7:e<sup>-</sup>.<sup>32</sup> It is evident that the contact resistance becomes negligibly small when  $N_e$  exceeds the critical concentration for an insulator-metal transition. This experimental finding demonstrates that a high carrier concentration in the support is needed to induce effective electron donation, in addition to the requirement that  $\phi_M - \phi_{\text{semi}} > 0$ . The high  $N_e$  region of the support has enough on contact with the transition metal particles for smooth electron transfer. This concept of effective electron transfer from a support/promotor to a loaded metal was also verified for ethanol synthesis by

catalytic hydrogenation of CO, which is isoelectronic with N<sub>2</sub>.<sup>35</sup>

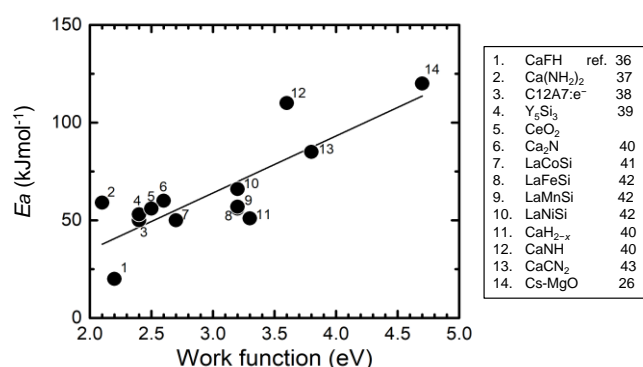


Fig.12 Correlation between activation energy for NH<sub>3</sub> synthesis and work function of support materials for Ru.

Figure 12 shows the correlation between the work function ( $\phi$ ) of various active supports and the activation energy ( $E_a$ ) for NH<sub>3</sub> synthesis. The  $\phi$  of the active support is distinctly reduced when an anion vacancy trapping an electron is created by heating or metal loading. It is noted that the  $E_a$  decrease with the work function of the support is a general trend, indicating that this is a guideline for seeking active supports for low-temperature NH<sub>3</sub> synthesis.

Recently a novel promotion effect was reported, spin effect by ferromagnetic metal.<sup>28</sup> The activation energy would be reduced by a difference energy between up and down-spin band. Since the Curie temperature of Co is high (1115°C for bulk), ferromagnetic state would be retained at NH<sub>3</sub> synthesis temperature. An experimental examination is waited for the real catalyst.

### 3.3. Electride catalysts

An electride is a material in which electrons serve as anions and may be regarded as a crystalline form of solvated electrons.<sup>44</sup> Since an anionic electron has no nucleus, unlike a conventional anion, it is loosely bound in the electride. Thus, electride materials intrinsically have low work functions. In this section, electride-based catalysts for NH<sub>3</sub> synthesis are described.

#### 3.3.1 C12A7:e<sup>-</sup>

After the discovery of electrides in 1982 by Dye,<sup>45</sup> a long-standing issue was the realization an electride stable under ambient conditions. The first RT stable electride was synthesized using 12CaO·7Al<sub>2</sub>O<sub>3</sub> (abbreviated as C12A7) with a 3-dimensionally connected cage structure in which O<sup>2-</sup> ions are accommodated as counter anions. Extraction of

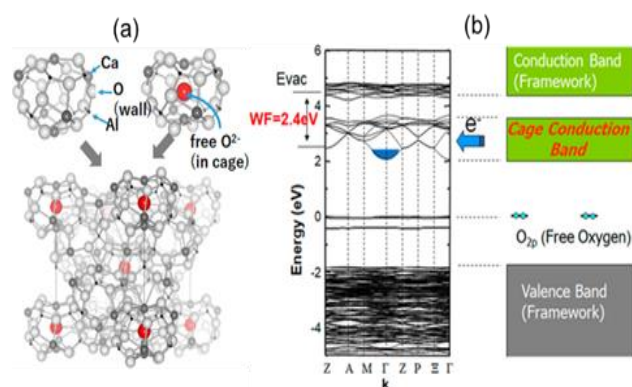


Fig.13 Structure of C12A7 (a) crystal structure, Red ball denotes O<sup>2-</sup> accommodated in the cage as the counter anion to compensate the positive charge of the cage wall. C12A7:e<sup>-</sup> is obtained by exchanging these O<sup>2-</sup> with electron. (b) Band structure of C12A7:e<sup>-</sup>. In-cage O<sup>2-</sup> loosely bounded by the cage is extracted, electrons are injected to the cage conduction band, thereby the sample becomes conducting and exhibits low work function.

these O<sup>2-</sup> ions leads to the injection of anionic electrons into the positively charged cages.<sup>46</sup> The resulting electride C12A7:e<sup>-</sup> (Fig. 13) is chemically stable and has a work function of 2.4eV,<sup>38</sup> which is comparable to that of potassium metal. A low work function and chemical/thermal stability are not compatible in general. The primary origin for this unique combination in C12A7:e<sup>-</sup> is the entrapment of anionic electrons in the cages whose open mouths are too small for H<sub>2</sub>O/O<sub>2</sub> to penetrate, preventing them from entering inside through the cage walls. Thus, the electronic properties are governed by anionic electrons in the cages, while the thermal properties are controlled by the Ca-Al-O network structure. While alkali metals have low work functions, they are chemically sensitive to the atmosphere and have low melting points (high vapor pressures), so their application as promoters is not practical. C12A7:e<sup>-</sup> compensates these shortcomings.

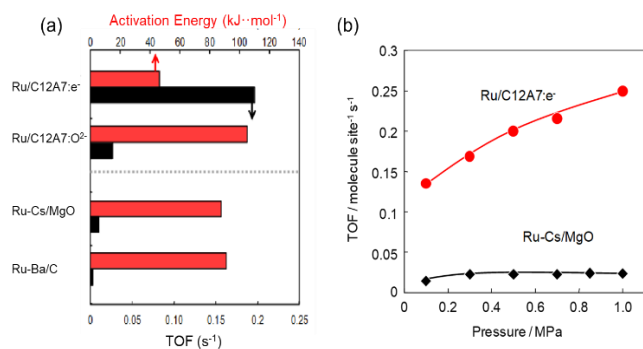


Fig.14 (a) TOF (360°C, 0.1 MPa) and apparent activation energies of various supported Ru (2wt%) catalysts. C12A7:e<sup>-</sup>: electride with  $2 \times 10^{21} \text{ cm}^{-3}$  electron, C12A7:O<sup>2-</sup>: electron-free, O<sup>2-</sup> is located in the cage as a counter anion. (b) Pressure dependence of TOF.  $\text{H}_2/\text{N}_2=3$ .<sup>26</sup>

Ru-loaded C12A7:e<sup>-</sup> exhibits high activity at mild conditions<sup>26</sup> as shown in Fig.14(a); the activation energy is reduced to almost half, and the TOF is higher by an order of magnitude compared with Ru-Cs/MgO. In addition, this catalyst is insensitive to H-poisoning (Fig.14b), which is thought to be a common drawback of Ru catalysts. Kinetic analysis based on nitrogen isotopic exchange experiments revealed the N<sub>2</sub> dissociation is no longer the rate determining step, due to enhanced electron donation to the N<sub>2</sub> adsorbed on Ru.<sup>47</sup> The mechanism for insensitivity to H<sup>-</sup> poisoning was suggested from an experimental comparison of H-absorption of Ru-loaded and Ru-free C12A7:e<sup>-</sup> samples. Ru-free C12A7:e<sup>-</sup> converts into C12A7:H<sup>-</sup> via reactions of electrons in the cages with H<sub>2</sub> at the temperatures relevant for NH<sub>3</sub> synthesis. Since C12A7:H<sup>-</sup> is more stable than C12A7:e<sup>-</sup>, H-incorporation into C12A7:e<sup>-</sup> monotonically proceeds with time. However, the situation rather differs for the same sample heating in H<sub>2</sub> + N<sub>2</sub> atmosphere as shown in Fig.15, i.e., the H incorporation into the sample is very limited and easily saturate with time. This striking difference indicates hydrogenation occurs only near the surface of Ru/C12A7:e<sup>-</sup>, and a H<sup>0</sup> adatom generated by H<sub>2</sub> dissociation on Ru reacts with an electron in the cage on the surface/near surface region, and H<sup>-</sup> is formed in the cage. When an N adatom comes to the periphery of a Ru nanoparticle, the H<sup>-</sup> escapes from the cage as H<sup>0</sup> with smaller size (smaller than H<sup>-</sup> by half) to react with the N atom to form a N-H bond, leaving an electron in the cage. As a consequence, the coverage of the active site on the Ru nanoparticles with hydrogen can be suppressed. The reactions described above are expressed in the following:

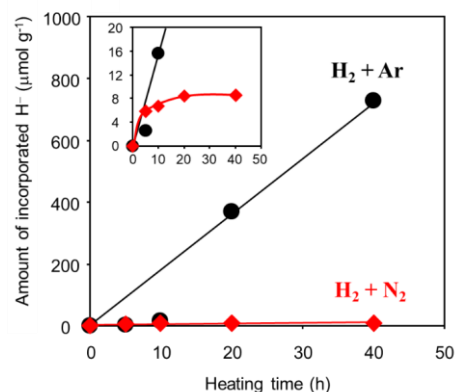
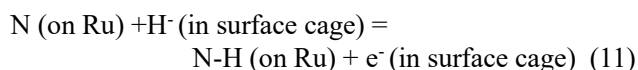
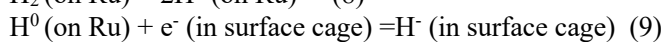


Fig.15 Amount of incorporated H ions in Ru/C12A7:e<sup>-</sup> after heat treatment in H<sub>2</sub> atmosphere (75 kPa) and Ar (25 kPa) gas flow at 633 K. Red diamond: Ru/C12A7:e<sup>-</sup> heated in H<sub>2</sub> (75 kPa) and N<sub>2</sub> (25 kPa) gas flow at 633 K. Inset shows the enlarged profiles.<sup>47</sup>

### 3.3.2 Extension of electride catalysts

The analysis of the results on the Ru/C12A7:e<sup>-</sup> system reveals the essence of the electride catalyst: the presence of a high concentration of low work function electrons at/near the periphery of loaded metal particles, combined with fast reactions of (1) H adatoms and these electrons to form H<sup>-</sup> anions, and (2) the resulting H<sup>-</sup> anions and N adatoms to form a N-H bonds. This idea leads to the hypothesis that if the work function of the anionic electrons is low and the related band crosses the Fermi level, such a material would work as a good active support for NH<sub>3</sub> synthesis. Following this idea, a search was performed based on the assumption that band structures similar to that of C12A7:e<sup>-</sup> should exist near the surface for some category of materials. This idea led to the concept of the surface electride.<sup>44,48</sup> Monovalent

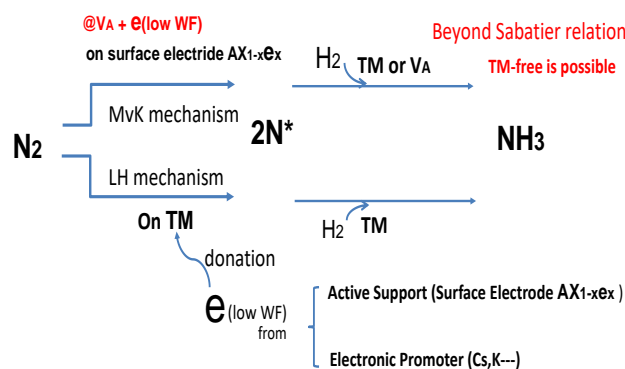


Fig.16 Contribution of surface electride to two routes for N<sub>2</sub>-activation

anions with metal cations have less binding and lattice cohesive energy, in general. Thus, we focused on metal hydrides and amines as the candidates for surface electrified. This resulted in our discovery of the Ru-Ba / Ca (NH<sub>2</sub>)<sub>2</sub> catalyst,<sup>49</sup> which has the highest activity to date. The high concentration of electrons trapped at the anion vacancy sites in an electrified may be discriminated from the F-center as a point defect. An F-center is isolated with each other such defects in general and thus does not produce itinerant electrons. This difference endows electrifieds with low work functions and itinerant electron nature. Figure 16 summarizes the contribution of surface electrified to two kinds of N<sub>2</sub> activation routes (LH and MvK mechanisms).

Also, the parent materials for electrifieds were extended from ionic insulators with open bandgaps to intermetallic compounds in which high electron densities populate crystallographic void sites, and new catalysts were searched for. One such intermetallic electrified is LaCoSi,<sup>41</sup> which exhibits the highest activity and the lowest activation energy among the Co-supported catalysts reported so far. Figure 17 summarizes the progress in electrified materials and electrified catalysts for NH<sub>3</sub> synthesis.

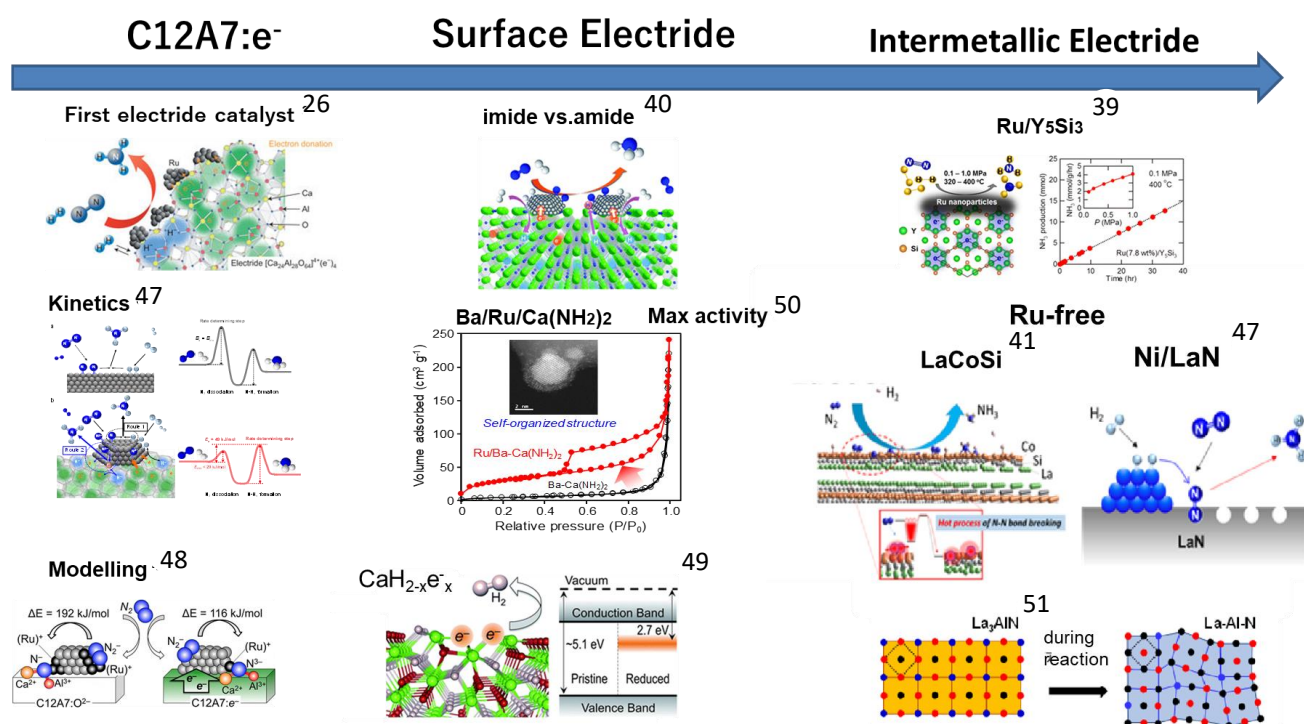


Fig. 17 Progress in electrified-based catalysts for NH<sub>3</sub> synthesis. Number shows reference

Cesium is well known as an effective electronic promoter for NH<sub>3</sub> synthesis but the action mechanism appears to be still elusive, particularly its actual chemical state. In many cases, cesium is added in the form of the nitrate, carbonate or hydroxide, but these compounds cannot be reduced to cesium metal as a low work function material (2.1 eV) under NH<sub>3</sub> synthesis conditions. The formation of stable suboxides during the reaction process is plausible. Recently, we reported that Cs<sub>3</sub>O is an electrified, which may be described as (Cs<sup>+</sup>)<sub>3</sub>(O<sup>2-</sup>)(e<sup>-</sup>). It in fact has lower work function (1.7 eV) than Cs metal.<sup>32</sup> This is also true for Cs<sub>11</sub>O<sub>5</sub>. The formation of suboxide electrifieds thus appears to be the origin of electron promotion by addition of alkali and

alkaline earth metal salts.

#### 4. Next Challenges

In the last decade, much progress has been made in catalysts for green ammonia synthesis, making it possible to shift the rate determining step from N<sub>2</sub> dissociation to N-H bond formation. As a result, the next technical challenges to be overcome for sustainable nitrogen activation becomes clear. Here several challenges are

raised from the viewpoint of catalytic N<sub>2</sub> activation for applications.

- Catalyst for N-H bond formation

It is now clear that the rate determining step in NH<sub>3</sub> formation is the creation of N-H bonds, in particular NH + H → NH<sub>2</sub> for advanced catalysts<sup>42</sup> that greatly reduce the barrier of N<sub>2</sub> dissociation. What is an appropriate catalyst to efficiently execute this process?

- Ru-free & chemically stable catalyst with high activity

There are two major obstacles for catalysts for green NH<sub>3</sub> synthesis. All of the highly active catalysts described to date depend on Ru, which is a precious metal. While active catalysts with non-precious transition metals have been reported, their ammonia formation rate is lower than that of the Ru-loaded samples.<sup>29,50</sup> The other issue is the high sensitivity of active catalysts to the ambient atmosphere. The alkaline earth amides, hydrides, and rare-earth nitrides are not exceptions. Since catalyst shaping is indispensable for industrial applications, it is extremely critical that the catalysts materials exhibit sufficient chemical inertness to withstand this procedure.

An approach to solving this issue is to utilize a property changeable material during ammonia synthesis. In this case, a starting material which is chemically insensitive to the ambient atmosphere is used. Such a material is mostly inactive or less active as a catalyst, but some of it is converted to a highly active form by reaction with hydrogen during ammonia synthesis. An example is Ni loaded on La<sub>3</sub>AlN with the inverse perovskite structure.<sup>51</sup> This material is chemically inert in conventional atmosphere and is converted to rock salt-type La (Al)N during ammonia synthesis. The resulting catalytic material exhibits high activity comparable to Ni/LaN, whose activity is easily degraded upon exposure to the outside atmosphere. Although transition metal-free catalysts with high activity and chemical inertness are the goal of academic research, no such a catalyst has been realized to date as far as I know.

- Efficient direct reduction of N<sub>2</sub> with H<sub>2</sub>O as a H source<sup>52</sup>

This scheme is possible using metal complex catalysts and electrocatalysis. However, a large amount of reducing agent is required for the former, and the current efficiency is very low due to competition from hydrogen evolution.

- Direct synthesis of nitrogen-bearing fine chemicals from N<sub>2</sub><sup>53</sup>

There are many nitrogen-bearing molecules which are value-added chemicals. If such chemicals could be directly

synthesized from N<sub>2</sub> at mild conditions, the benefits should be huge.

### Acknowledgements

This research was supported by a JST-Mirai Program (JPMJMI21E9) and a NEDO Project (JPNP21012). The author thanks Profs. Masaaki Kitano (Tokyo Tech) and Daniel Fredrickson (Wisconsin-Madison) for their helpful discussion.

### References

1. L.R.Jennings (ed.), Catalytic Ammonia Synthesis, Springer Science & Business Media, 1991
2. H.Liu, Ammonia synthesis catalysts: innovation and practice. World Scientific.2013
3. A.V-Medina and R.B-Alcantara, Techno-economic challenges of green ammonia as an energy vector. Academic Press.2020.
4. K.I.Aika, and H.Kobayashi, (Eds.). CO<sub>2</sub> Free Ammonia as an Energy Carrier: Japan's Insights. Springer Nature, 2022.
5. R.Schlögl, R. Angewandte Chemie International Edition, **2003**, 42, 2004; A.Mittasch and W.Frankenburger, J.Chem.Edu, **1929**, 6, 2097.
6. A.Ozaki, Accounts of Chemical Research, **1981**,14,16.
7. J.G.Chen et al. Science, **2018**, 360, eaar6611.
8. Q.Wang, J.Guo and P.Chen, Journal of Energy Chemistry, **2019**, 36, 25.
9. C.D.Z-Yazdi, J.S.Hargreaves, S.Laassiri and R.A.Catlow, Royal Society open science, **2021**, 8, 210952.
10. P.Mehta et al. Nature Catalysis, **2018**, 1, 269.
11. L. R Winter and J.G. Chen, Joule, **2021**, 5, 300.
12. Y.Liu et al. Journal of Materials Chemistry A, **2021**, 9, 6694.
13. Y.Wei, W.Jiang, Y.Liu, X. Bai, D.Hao and B.J.Ni Nanoscale, **2022**, 14, 2990.
14. T.Oshikiri, K.Ueno and H.Misawa, Angewandte Chemie, **2014**, 126, 9960.
15. A.W.Tricker et al. ACS Energy Lett. **2020**, 5,3362.
16. G.F.Han et al. Nature Nanotechnology, **2021**,16, 325.
17. C.He et al. ACS Sustainable Chemistry & Engineering, **2022**, 10, 746.
18. Q.Lai et al. Science Bulletin, **2022**, 67, 2124.
19. P.Wang et al. Nat.Chem. **2017**,9,64
20. M.J.Bezdek and P.J. Chirik, **2019**, Nature 568,464.
21. Y.Ashida et al. Nature **2019**,568, 536
22. A. V. Krylova and E. Ch. Jenikejev, Chem. Tech.**1963**, 15,23114.
23. R.Kojima and K.I.Aika, Chemistry Letters, **2000**, 29, 514.
24. C.J.Jacobsen et al. Journal of the American Chemical Society, **2001**,123, 8404.
25. D.McKay et al. Chem.Comm. **2007**, 7,3051.
26. M.Kitano et al. Nature chemistry, **2012**, 4, 934.
27. T.Ye et al. Nature, **2020**, 583, 391.
28. A.Cao et al. Nat.Comm. **2022**,13,2382.
29. F.Chang et al. Nature Catalysis, **2022**, 5, 222.
30. C.D.Z-Yazdi, J.S. Hargreaves and C.R.A.Catlow, Journal of Physical Chemistry C, **2015**,119, 28368.
31. C.D.Z-Yazdi, J.S. Hargreaves and C.R.A.Catlow, Journal of Physical Chemistry C, **2018**, 122, 6078.
32. H.Hosono, Catalysis Letters, **2022**, 152, 307.
33. S.Kanbara et al. Journal of the American Chemical Society, **2015**, 137, 14517.
34. S-W.Kim et al. Nano Letters, **2007**, 7, 1138.

35. H.Sugiyama et al. Journal of Physical Chemistry Letters, **2023**,14, 1259.
36. M.Hattori et al. Nature Com. (2020)11,2001
37. M.Kitano et al. Angewandte Chemie International Edition, **2018**, 57, 2648.
38. Y.Toda et al. Advanced Materials, **2007**, 19, 3564.
39. Y.Lu et al. Journal of the American Chemical Society, **2016**,138,3970.
40. M.Kitano et al. Chemical Science, **2016**,7, 4036.
41. Y.Gong et al., Nature catalysis, **2018**, 1, 178.
42. Y.Gong et al. J.Amer.Chem.Soc. **2022**, 144. 8683.
43. K.Kishida et al. ACS Applied Energy Materials, **2020**, 3, 6573.
44. H.Hosono and M.Kitano, Chemical Reviews, **2021**,121, 3121.
45. D.L.Dye, Science, **1990**, 247, 663.
46. S.Matsuishi et al. Science, **2003**, 301, 626.
47. M.Kitano et al. Nat.Commun.**2015**, 6, 6731.
48. N.Kuganathan, H.Hosono, A.I.Shluger and P.V.Sushko, Journal of the American Chemical Society, **2014**, 136, 2216.
49. P.V.Ong, L.E. Johnson, H.Hosono and P.V.Sushko, Journal of Materials Chemistry A, **2017**, 5, 5550.
50. M.Kitano et al. Angewandte Chemie International Edition, **2018**, 57, 2648.
51. Y.Lu et al. Angewandte Chemie International Edition, **2022**, 61, e202211759.
52. X.Cui, C.Tang and Q. Zhang, Advanced Energy Materials, **2018**, 8, 1800369.
53. S.Kim, F.Loose and P.J. Chirik, Chemical reviews, **2020**, 120, 5637